Contribution from the Department of Chemistry,
Iowa State University, Ames, Iowa 50011

Formation of Unexpected Silicon Alkoxide Isomers in a Rectangular Planar Chelating Framework

B. de Ruiter, J. E. Benson, R. A. Jacobson, and J. G. Verkade*

Received October 12, 1989

Reaction of the tetraols $(HOCH_2)_2C(CH_2)_nC(CH_2OH)_2$ (**4**, $n = 1$; **5**, $n = 3$) with $(MeO)_3SiMe$ in the presence of base is facilitated by the absence of solvent. The polymeric intermediate from the reaction involving **1** partially depolymerizes when heated under vacuum to give a pair of stable tetracyclic isomers **6a,b** as sublimates. In **6a** the MeSiOSiMe moiety spans the rectangular array of alkoxy oxygens such that the CSiOSiC plane of this group is parallel with the hydrocarbon three-membered ring, while in **6b** it is perpendicular to the ring. Depolymerization of the intermediate from the reaction involving **5** gives a tricyclic product in which an MeSi group spans three alkoxy oxygens. The structures of of **6a**, **6b**, and **7** were determined by X-ray crystallography.

Introduction

Polycyclic esters of silicon such as **1**[1] and **2**[2] have been known for many years. In an attempt to synthesize esters of type **3**,

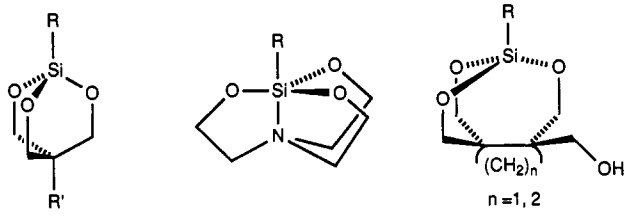

1 **2** **3**

however, we were surprised to find that (a) reaction 1 gave the isomeric disiloxanes, **6a** and **6b**, whereas reaction 2 afforded the

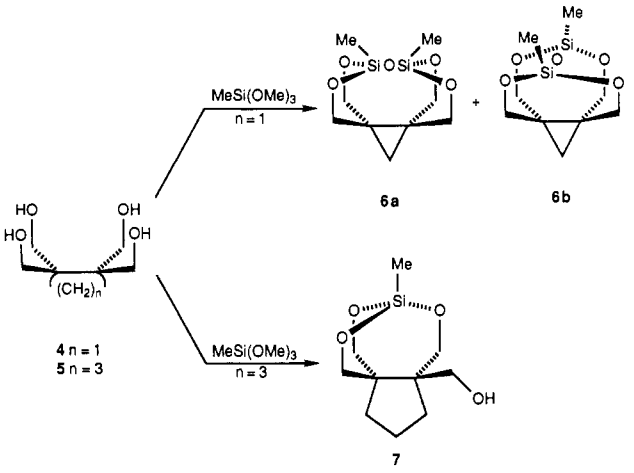

expected monosilyl ester **7**, (b) both reactions afforded the products in the absence of solvent, and (c) the use of a solvent for the reactions gave only polymer, even under conditions of high dilution.

Experimental Section

1,3-Dimethyl-2,4,10,11,13-pentaoxa-1,3-disilatetracyclo[6.2.2.0^{6,8}.2^{3,6}]tetradecane (6a) and 1,3-Dimethyl-2,4,10,11,13-pentaoxa-1,3-disilatetracyclo[6.2.2.0^{6,8}.2^{1,6}]tetradecane (6b). To 2.72 g (20.0 mmol) of $MeSi(OMe)_3$ was added under N_2 a mixture of **4**[3] (3.24 g, 20.0 mmol) and NaOMe (0.28 g, 5.2 mmol). Gradual heating under N_2 to 85 °C produced MeOH, which was distilled off at atmospheric pressure. After 2 h at 85 °C, the heat source was removed and the flask evacuated, leaving a brittle foamy solid, from which 1.13 g of material sublimed over a temperature range of 100–200 °C (0.3 Torr). Extraction of the sublimate with Et_2O left 0.68 g of insoluble **1**. Evaporation of the ether solution and sublimation of the residue at 90 °C/0.2 Torr gave 260 mg of sublimate, which upon recrystallization from Et_2O gave 140 mg of a mixture of **6a,b**. A second crop of crystals (95 mg) consisted of almost pure **6b**. Two additional recrystallizations gave pure **6b** (mp 132–135 °C; ^1H NMR ($CDCl_3$) δ 0.18 s ($SiCH_3$), 1.09 s (ring CH_2), 3.93 d and 4.44 d (AB quartet, ^1J(H-H) = 12.3 Hz, OCH_2); ^{13}C NMR ($CDCl_3$) δ −5.7 q (^1J(C-H) = 120.3 Hz, SiC), 31.7 t (^1J(C-H) = 162.0 Hz, ring CH_2), 36.5 s (ring C), 72.1 t (^1J(C-H) = 146.6 Hz, OC); MS (70 eV) *m/e* (relative intensity) 260 (M, 26), 245 (M − CH_3, 30), 135 (M − $C_7H_9O_2$, 100)). Sublimation of the residue remaining after evaporation of the original ether extract between 90 and 190 °C gave crude **6a**, which upon one recrystallization from ether yielded 120 mg of pure compound (mp 207–210 °C; ^1H NMR ($CDCl_3$) δ 0.22 s ($SiCH_3$), 0.59 s (ring CH_2), 3.82 d and 4.50 d (AB quartet, ^2J(H-H) = 11.1 Hz, OCH_2); ^{13}C NMR ($CDCl_3$) δ −5.4 q (^1J(C-H) = 120.6 Hz, SiC), 15.1 t (^1J(C-H) = 161.4 Hz, ring CH_2), 31.7 s (ring C), 66.9 t (^1J(C-H) = 147.3 Hz, OC); MS (70 eV) *m/e* (relative intensity) 260 (M, 12), 245 (M − CH_3, 21), 135 (M − $C_7H_9O_2$, 100)).

1-Methyl-4-(hydroxymethyl)-2,10,11-trioxa-1-silatricyclo[6.2.2.0^{4,8}]dodecane (7). To 2.94 g (21.6 mmol) $MeSi(OMe)_3$ was added under N_2 a mixture of 3.80 g (20.0 mmol) of **5**[4] and 0.27 g (5.0 mmol) NaOMe. According to the same procedure given in the above preparation for the sublimation of product from the polymeric intermediate, 3.56 g of sublimate was extracted with Et_2O. The sublimation residue was also extracted with ether. The combined extracts upon evaporation deposited 3.54 g of nearly pure **7** in 77% yield, which was recrystallized from Et_2O to a melting point of 110.5–112 °C in 53% yield (^1H NMR ($CDCl_3$) δ 0.24 s ($SiCH_3$), 1.2–2.0 m (ring CH_2), 2.12 t (OH), 3.55–4.3 m (OCH_2); ^{13}C NMR ($CDCl_3$) δ −7.7 (SiC), 20.7, 30.3, and 32.4 (ring CH_2), 52.4 and 55.5 (quaternary C), 62.3, 65.4, 68.1, and 72.8 (OC); MS (16 eV) *m/e* (relative intensity) 230 (M, 0.4), 212 (M − H_2O, 34), 200 (M − CH_2O, 100)).

Table I. Summary of Crystal Data for **6a**, **6b**, and **7**

	6a	**6b**	**7**
formula unit	$Si_2O_5C_9H_{16}$	$Si_2O_5C_9H_{16}$	$SiO_4C_{10}H_{18}$
space group	$P2_1/a$	Cc	$C2/c$
a, Å	10.790 (2)	10.144 (2)	27.007 (4)
b, Å	14.629 (4)	7.866 (2)	6.350 (3)
c, Å	7.600 (2)	15.503 (4)	15.157 (8)
β, deg	91.36 (4)	105.02 (2)	124.95 (3)
V, Å^3	1199.4 (5)	1194.8 (5)	2130 (2)
Z	4	4	8
d_{calcd}, g cm^{-3}	1.442	1.447	1.436
μ, cm^{-1}	2.96	2.95	1.89
T, K	295	295	295
λ, Å (Mo Kα)	0.709 26	0.709 26	0.079 26
scan mode	ω	ω	ω
$2\theta_{max}$, deg	50	50	50
no. of reflns, measured	4755	2465	4399
no. of reflns, obs ($I > 3\sigma_I$)	2685	1250	2211
no. of unique reflns	1392	626	1221
R^a	0.070	0.043	0.068
$R_w{}^b$	0.081	0.042	0.077

$^a R = \sum||F_o| - |F_c||/\sum|F_o|$. $^b R_w = [\sum w(|F_o| - |F_c|)^2/\sum w|F_o|^2]^{1/2}$, where $w = 1/\sigma_F{}^2$.

(1) Rathke, J. W.; Guyer, J. W.; Verkade, J. G. *J. Org. Chem.* **1970**, *35*, 2310.
(2) Voronkov, M. G.; Dyakov, V. M.; Kirpichenko, S. V. *J. Organomet. Chem.* **1982**, *233*, 1 and references cited therein.
(3) Buchta, E.; Kroeniger, A. *Chimia* **1968**, *22*, 430.
(4) Weinges, K.; Klessing, K.; Kolb, R. *Chem. Ber.* **1973**, *106*, 2298.

0020-1669/90/1329-1065$02.50/0

Table II. Positional Parameters[a] (×10⁴) for **6a**

atom	x	y	z	U_{eq},[b] Å²
Si1	788	2452 (6)	7188	40 (2)
Si2	−622 (2)	2510 (6)	5196 (1)	38 (2)
O1	2150 (13)	1335 (15)	7157 (10)	50 (5)
O2	−252 (15)	1379 (15)	7521 (9)	49 (4)
O3	474 (16)	1137 (16)	4855 (9)	49 (4)
O4	−1905 (14)	1312 (16)	5211 (10)	44 (5)
O5	145 (19)	3203 (4)	6183 (12)	41 (1)
C1	2001 (21)	−551 (24)	6997 (13)	50 (6)
C2	−150 (20)	−529 (24)	7427 (11)	45 (6)
C3	490 (20)	−942 (17)	6684 (12)	47 (6)
C4	−311 (20)	−1020 (20)	5708 (13)	40 (6)
C5	446 (23)	−553 (24)	5026 (13)	70 (7)
C6	−1786 (17)	−358 (25)	5492 (13)	52 (5)
C7	192 (30)	−2646 (8)	6205 (20)	54 (4)
C8	1387 (24)	4398 (27)	7958 (12)	56 (6)
C9	−1013 (26)	4186 (29)	4465 (13)	56 (7)
H11	240	−119	758	76
H12	243	−88	649	76
H21	−111	−107	730	76
H22	47	−102	804	76
H31	147	−98	527	76
H33	−1	−121	444	76
H41	−240	−114	498	76
H42	−217	−48	607	76
H71	97	−335	608	76
H72	−52	−345	640	76
H81	53	511	795	76
H82	181	389	860	76
H83	209	503	772	76
H91	−13	495	445	76
H92	−170	510	467	76
H93	−149	385	380	76

[a] The estimated standard deviations in the parentheses are for the least significant digits. Parameters for hydrogen atoms are multiplied by 10^3. [b] $U_{eq} \equiv 10^3/3\sum U_{ij}\vec{a}_i^*\cdot\vec{a}_j^*\mathbf{a}_i\mathbf{a}_j$, where the temperature factors are defined as $\exp(-2\pi^2\sum \mathbf{h}_i\mathbf{h}_j\mathbf{a}_i^*\mathbf{a}_j^*\mathbf{U}_{ij})$.

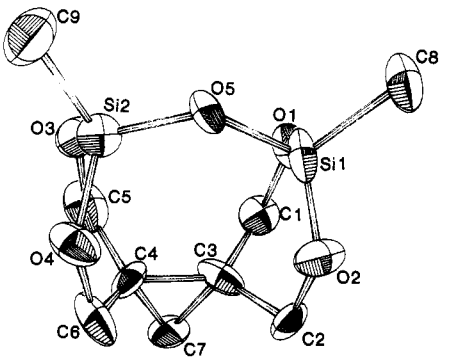

Figure 1. ORTEP drawing of **6a**, with ellipsoids drawn at the 50% probability level.

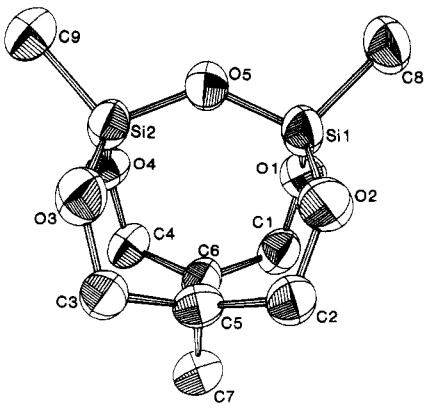

Figure 2. ORTEP drawing of **6b**, with ellipsoids drawn at the 50% probability level.

Crystal Structure Determinations. Relevant crystallographic data are given in Table I. A Syntex $P2_1$ diffractometer was used for all data collection. Initial indexing was carried out by an automatic indexing technique. The resulting cell dimensions and monoclinic symmetry were confirmed by examining axial photographs.

The intensity data were corrected for Lorentz–polarization effects; absorption corrections were not deemed necessary ($\mu < 3.0$ cm^{-1}), and no decay was observed. The estimated variance in each intensity was calculated by $\sigma_I^2 = C_T + C_B + (0.03C_T)^2 + (0.03C_B)^2$, where C_T and C_B represent the total and background counts, respectively. Computer programs used in this study are detailed in ref 5.

The positions of the atoms were determined by use of the direct methods program MULTAN. Hydrogen atoms were included but not refined. Positional and thermal parameters were refined initially by

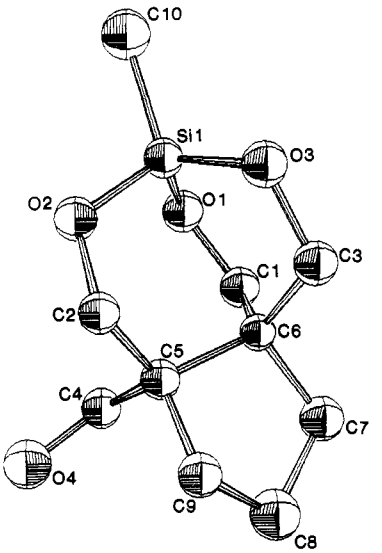

Figure 3. ORTEP drawing of **7**, with ellipsoids drawn at the 50% probability level.

Scheme I

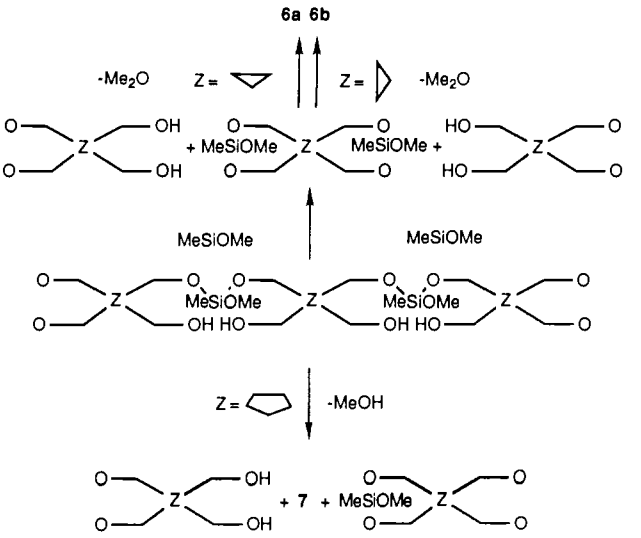

(5) Calculations were carried out on a VAX 11/780 computer. The indexing of the crystal was done by using the program BLIND (Jacobson, R. A. *J. Appl. Crystallogr.* **1976**, *9*, 115). Structure factor calculations and least-squares refinements were done by using the block-matrix/full-matrix program ALLS (Lapp, R. L.; Jacobson, R. A. U.S. Department of Energy Report IS-4078; Iowa State University: Ames, IA, 1979), Fourier series calculations were done by using the program FOUR (Powell, D. R.; Jacobson, R. A. U.S. Department of Energy Report IS-4737; Iowa State University: Ames, IA, 1980), and molecular drawings were created by using the program ORTEP (Johnson, C. K. U.S. Atomic Energy Commission Report ORNL-3794; Oak Ridge National Laboratory: Oak Ridge, TN, 1970). The direct methods program used was MULTAN 80 (Main, P.; Fiske, S. J.; Hull, S. E.; Lessinger, L.; Germain, G.; Declercq, J.-P.; Woolfson, M. M. University of York: York, England, 1980).

Table III. Positional Parameters[a] (×10⁴) for **6b**

atom	x	y	z	U_{eq},[b] Å²
Si1	6940 (3)	4941 (2)	2733 (5)	61 (2)
Si2	8885 (3)	6365 (2)	3212 (4)	57 (2)
O1	7502 (8)	4525 (5)	953 (10)	81 (3)
O2	5757 (7)	5612 (6)	2256 (12)	71 (3)
O3	8009 (9)	7256 (5)	2833 (13)	87 (3)
O4	9639 (8)	6101 (7)	1463 (10)	65 (3)
O5	8034 (7)	5521 (5)	3774 (10)	68 (3)
C1	7542 (13)	4966 (8)	−707 (17)	56 (5)
C2	5648 (11)	6244 (8)	827 (17)	70 (4)
C3	7371 (12)	7457 (7)	1208 (17)	64 (4)
C4	9193 (11)	6190 (9)	−339 (15)	56 (4)
C5	6921 (11)	6652 (8)	155 (16)	62 (4)
C6	7838 (11)	5958 (8)	−582 (15)	55 (4)
C7	7110 (12)	6619 (9)	−1812 (18)	66 (5)
C8	6394 (13)	3998 (9)	4149 (19)	83 (5)
C9	9987 (13)	6651 (9)	5045 (18)	70 (5)
H11	662	492	−132	76
H12	816	465	−150	76
H21	510	677	119	76
H22	527	588	−24	76
H31	801	781	38	76
H32	663	791	144	76
H41	970	577	−111	76
H42	932	688	−71	76
H71	753	718	−233	76
H72	639	636	−258	76
H81	541	404	418	76
H82	673	414	546	76
H83	669	340	371	76
H91	1021	733	499	76
H92	962	644	621	76
H93	1082	625	480	76

[a] The estimated standard deviations in the parentheses are for the least significant digits. Parameters for hydrogen atoms are multiplied by 10^3. [b] $U_{eq} \equiv 10^3/3\sum U_{ij}\bar{a}_i^*\cdot\bar{a}_j^*\mathbf{a}_i\mathbf{a}_j$, where the temperature factors are defined as $\exp(-2\pi^2\sum \mathbf{h}_i\mathbf{a}_i^*\mathbf{a}_j^*U_{ij})$.

Table IV. Positional Parameters[a] (×10⁴) for **7**

atom	x	y	z	U_{eq},[b] Å²
Si1	1017 (1)	1251 (4)	8602 (2)	32 (1)
O1	745 (2)	3600 (10)	8208 (3)	38 (3)
O2	1765 (2)	1371 (9)	9471 (3)	33 (2)
O3	731 (3)	348 (9)	9212 (4)	39 (3)
O4	2567 (3)	6142 (11)	11023 (5)	51 (3)
C1	634 (3)	4821 (14)	8881 (6)	35 (4)
C2	1962 (4)	1893 (13)	10503 (6)	35 (5)
C3	737 (5)	1740 (13)	9954 (8)	53 (8)
C4	1890 (3)	5843 (13)	10253 (6)	38 (4)
C5	1690 (3)	3930 (13)	10602 (5)	27 (3)
C6	1015 (4)	3929 (12)	10045 (6)	32 (5)
C7	905 (4)	5380 (16)	10734 (7)	48 (6)
C8	1466 (4)	5784 (15)	11707 (6)	48 (5)
C9	1934 (5)	4136 (14)	11796 (7)	50 (7)
C10	854 (3)	−432 (15)	7511 (6)	43 (4)
H11	17	471	856	76
H12	74	639	888	76
H21	244	207	1097	76
H22	185	65	1082	76
H31	100	104	1073	76
H32	30	194	972	76
H41	178	560	949	76
H42	168	718	1030	76
H71	62	460	1089	76
H72	70	677	1032	76
H81	145	559	1238	76
H82	162	731	1173	76
H91	189	272	1209	76
H92	236	472	1225	76
H101	123	−59	750	76
H102	71	−191	759	76
H103	50	25	677	76

[a] The estimated standard deviations in the parentheses are for the least significant digits. Parameters for hydrogen atoms are multiplied by 10^3. [b] $U_{eq} \equiv 10^3/3\sum U_{ij}\bar{a}_i^*\cdot\bar{a}_j^*\mathbf{a}_i\mathbf{a}_j$, where the temperature factors are defined as $\exp(-2\pi^2\sum \mathbf{h}_i\mathbf{a}_i^*\mathbf{a}_j^*U_{ij})$.

block-matrix and finally by full-matrix least squares. The atomic scattering factors used were from ref 6. The final positional parameters are listed in Tables II–IV, and ORTEP drawings of **6a**, **6b**, and **7** are given in Figures 1–3, respectively.

Molecular Mechanics Calculations on 6a and 6b. These calculations were carried out with Version 2.0 of PCMODEL,[7] which contains all the necessary parameters for these molecules.

Discussion

Heating equimolar amounts of $MeSi(OMe)_3$ and **4** in the presence of NaOMe gives rise to a brittle highly insoluble solid, from which about 20% by weight sublimes, giving a mixture of **4** and a 1:1 ratio of isomers **6a** and **6b**. By contrast, the analogous reaction with **5** gives **7**.

Evidence that the volatile isomers **6a** and **6b** are formed in a thermolytic disproportionation of a polymer is that (1) no detectable amount of material could be extracted from this substance, even with pyridine, in which **4**, **6a**, and **6b** are soluble and (2) solution reactions of equimolar amounts of **4** and Cl_3SiMe in the presence of 3 equiv of pyridine in MeCH or THF led only to polymer under conditions of high dilution. A plausible pathway to **6a**, **6b**, and **7** is given in Scheme I. Interestingly, <5% yields of **6a**,**b** are realized when equimolar amounts of **4** and $[MeSi(OMe)_2]_2O$ are reacted at 170 °C. Under similar reaction conditions, $MeSi(OMe)_3$ and **5** afford a 77% yield of nearly pure **7**, while an analogous reaction of $[MeSi(OMe)_2]_2O$ and **5** gives this product in 39% yield.

Our results suggest that the closer approach of the alcohol arms in **5**, permitted by the larger hydrocarbon ring, compared with that in **4** accounts for the accommodation of one silicon bridgehead in **7** compared with two in a disilyloxy bridgehead system in **6a** and **6b**. The more open cages of **6a** and **6b** are favored by the narrow angles within the three-membered ring, which splay the alkoxy groups apart. This splaying effect stems from the wider CCC bond angles, which do not include C7 in **6a** and **6b** or C7, C8, and C9 in **7**. The average exocyclic CCC angles are 117.3(14), 117.6(10), and 113.6 (5)° in **6a**, **6b**, and **7**, respectively. The difference in these angles is not quite outside experimental error (i.e., 3 σ) between **6a** and **7**, but it is between **6b** and **7**.

Significant differences in the metrics of the structures of **6a** and **6b** occur only for their SiOSi bond angles (138.9 (9) and 132.9 (5)°, respectively) and their average SiOC bond angles (119.8 (11) and 126.4 (8)°, respectively). The former difference is made reasonable by the fact that in **6a** the SiOSi system is shared by two nine-membered rings, while the shared ring systems in **6b** are eight-membered. The smaller SiOC bond angles in **6a** can be attributed to the presence of these linkages in six-membered rings, while in **6b** the smallest rings in which these moieties reside are seven-membered, thus allowing the SiOC angles to widen. Molecular mechanics[7] calculations indicate that **6b** is only slightly more stable (by 1.19 kcal/mol) than **6a**.

Comparison of the average SiOC angle in the six-membered ring of **7** (117.0 (5)°) with that in **6a** (119.8 (11)°) reveals that they are the same within experimental error, as might be expected. Perhaps unexpectedly, the SiOC angle shared by the two seven-membered rings in **7** is only 114.5 (4)°. It should be noted that puckering in the five-membered hydrocarbon ring in **7** causes twisting around the C5–C6 bond, which in turn leads to a twist-pseudoboat conformation of the seven-membered rings, compared with the rigid pseudoboat conformations of the seven-membered rings in **6b**. While this conformational difference would not be expected to lead to such a large decrease in SiOC angle from the seven-membered rings of **6b** (126.4 (8)°) to those

(6) (a) Cromer, D. T.; Waber, J. T. *International Tables for X-ray Crystallography*; Kynoch Press: Birmingham, England, 1974; Vol. IV, Table 2.2a, pp 71–79. Hydrogen scattering factors were taken from: Stewart, R. F.; Davidson, E. R.; Simpson, W. T. *J. Chem. Phys.* **1965**, *42*, 3176. (b) Cromer, D. T.; Liberman, D. *International Tables for X-ray Crystallography*; Kynoch Press: Birmingham, England, 1974; Vol. IV, Table 2.3.1, pp 149–150.

(7) Available from Serena Software, Box 3076, Bloomington, IN 47402-3076.

of **7** (114.5 (4)°), it should be recalled that the three-membered hydrocarbon ring in **6b** widens the seven-membered ring pseudoboat, thus opening the SiOC angle.

It is interesting that the metric parameter with the greatest flexibility among these structures is the oxygen angle, since the Si-O bond distances (1.62-1.63 Å) and the OSiO angles (107-110°) appear to be quite constant within experimental error.

Acknowledgment. We are grateful to the National Science Foundation for support of this research and to Y. Su for assistance in the molecular mechanics calculations.

Supplementary Material Available: Tables of anisotropic thermal parameters, bond lengths, and bond angles for **6a**, **6b**, and **7** (9 pages); tables of calculated and observed structure factors for **6a**, **6b**, and **7** (11 pages). Ordering information is given on any current masthead page.

Contribution from Lash Miller Chemical Laboratories, Department of Chemistry, University of Toronto, Toronto, Ontario M5S 1A1, Canada, and AT&T Bell Laboratories, 600 Mountain Avenue, Murray Hill, New Jersey 07974

Liquid-Phase Metal Vapor Chemistry: Rotary Reactors and Electron-Beam Evaporation Sources

G. A. Ozin,*[,†] M. P. Andrews,*[,‡] C. G. Francis,[†] H. X. Hüber,[†] and K. Molnar[†]

Received March 21, 1989

A new rotatable metal atom reactor that allows electron-beam vaporizations of refractory materials into liquid solutions at reduced temperatures is described. This innovation demonstrably broadens the scope of synthesis from metal atoms and molecular high-temperature species. Details of the instrument and its operation are provided, together with results of studies of charged particle emissions, a description of techniques for quantifying the rate of metal atom deposition, and a description of a variable-temperature transfer tube for removing thermally labile compounds. A simple addition of the furnace that substantially reduces the power required to evaporate even the most refractory elements leads to dramatically increased vaporization rates for modestly powered 2-kW guns. The paper concludes with some test applications of the device in the liquid-phase electron-beam synthesis of some bis(η^6-arene) complexes of titanium, vanadium, and molybdenum.

1. Introduction

In his book on the condensed-phase reactions of high-temperature species, Klabunde[1] remarks on the need to perfect electron-beam equipment suitable for metal vapor synthesis (MVS). A notable innovation in this area has been the development of the reverse-polarity electron gun by Green and coworkers.[2] This device employs a positive hearth (anode) with an unearthed electrostatic focusing shield. With these modifications the primary (incident) electrons are focused on and confined by the positive hearth. Secondary electrons scattered from the molten metal are suppressed in numbers, with emission levels reduced by 3 orders of magnitude (milliamps to microamps). Reagent damage decreases as a result. Accompanying ion emissions from this device are small (microamps) and tolerable in a synthetic sense.[2]

Changing requirements in the field of metal vapor synthesis have stimulated efforts to extend the range of applicability of electron-beam technology to liquid-phase reaction chemistry, to quantify the metal atom deposition process, and to incorporate multivaporization sources in multimetallic applications.[3] In turn, these adaptations make the hardware more flexible for use in inorganic, organometallic, and materials synthesis.[3] This paper is an account of our efforts to meet these requirements. We first will sketch the basic features of the device to clarify the relationships between the design adaptations and their application. Following this, we will provide a description of the principle of operation of a work-accelerated, electrostatically focused electron gun. The information should be of interest to those unfamiliar with this technique of vaporization. This description will be followed by an evaluation of various electron gun characteristics, including power requirements and charged particle emissions. Our findings should be compared with those given by Green et al.[2] for static reactor systems. The paper concludes with some applications of the device in metal atom synthesis. Additional applications related more to materials science are elaborated in an article by Andrews.[3]

2. Elements of Electron Gun Design

Figures 1 and 2 show views of the dual electron gun, which is the subject of this paper.

2.1. Electron Gun Manifold. This manifold houses the cooling water and electrical connections for the electron gun hearths. The manifold is a hollow shaft constructed of highly polished stainless steel and supported rigidly and horizontally by the main flange assembly (Figure 1). An adjustable collar carries the majority of the weight of the gun as illustrated in Figure 1. A Teflon sleeve has been incorporated to allow easy sliding of the gun manifold through the collar to permit adjustments to the length of the gun.

2.2. Hearth Assembly. A detailed section of the dual gun is illustrated in Figure 2. The twin hearth furnace is constructed of copper and stainless steel. The metals to be vaporized are placed on the water-cooled copper hearths (10-mm diameter), which are capable of accepting 5-10 g of material. These hearths are threaded at the base and tighten against O-ring seals. This feature permits easy interchange of hearth designs. High-voltage feedthroughs connect the anodes through a 1-in.-thick glass-filled nylon insulation block. Half of this block provides additional insulation inside of the gun manifold. Vacuum tightness is achieved with O-ring flanges from the hearths to the nylon block, and from the nylon block to the end of the electron gun manifold. All water and electrical feedthroughs to the hearth assembly are electrically insulated from one another within the main electron gun manifold. Electrical and fluid-transfer leads exit collectively through a plastic sleeve in the rear of the unit (Figure 1).

The thoriated tungsten electron emitter filaments (cathodes) are positioned coaxially approximately 9 mm below the top of each hearth. Braided electrical leads pass from medium-current feedthroughs and, via ceramic insulators, make contact with the

[†] University of Toronto.
[‡] AT&T Bell Laboratories.

(1) Klabunde, K. J. *Chemistry of Free Atoms and Particles*; Academic Press: New York, 1980.
(2) Green, M. L. H. *J. Organomet. Chem.* **1980**, *200*, 119. Green, M. L. H.; O'Hare, D. In *High Energy Processes in Organometallic Chemistry*; Suslick, K., Ed.; ACS Symposium Series 333; American Chemical Society: Washington, DC, 1987.
(3) Andrews, M. P. In *Experimental Organometallic Chemistry*; Wayda, A. L., Darensbourg, M. Y., Eds.; ACS Symposium Series 357; American Chemical Society: Washington, DC, 1987.

0020-1669/90/1329-1068$02.50/0